




GPTMS-Modified Bredigite/PHBV Nanofibrous Bone Scaffolds with Enhanced Mechanical and Biological Properties

Monireh Kouhi^{1,2}  · Venugopal Jayarama Reddy^{2,3} · Seeram Ramakrishna²

Received: 15 August 2018 / Accepted: 5 November 2018 /

Published online: 20 November 2018

© Springer Science+Business Media, LLC, part of Springer Nature 2018

Abstract

Bioceramic nanoparticles with high specific surface area often tend to agglomerate in the polymer matrix, which results in undesirable mechanical properties of the composites and poor cell spreading and attachment. In the present work, bredigite (BR) nanoparticles were modified with an organosilane coupling agent, 3-glycidoxypropyltrimethoxysilane (GPTMS), to enhance its dispersibility in the polymer matrix. The polyhydroxybutyrate-co-hydroxyvalerate (PHBV) nanofibrous scaffolds containing either bredigite or GPTMS-modified bredigite (G-BR) nanoparticles were fabricated using electrospinning technique and characterized using scanning electron microscopy, transmission electron microscopy, and tensile strength. Results demonstrated that modification of bredigite was effective in enhancing nanoparticle dispersion in the PHBV matrix. PHBV/G-BR scaffold showed improved mechanical properties compared to PHBV and PHBV/BR, especially at the higher concentration of nanoparticles. In vitro bioactivity assay performed in the simulated body fluid (SBF) indicated that composite PHBV scaffolds were able to induce the formation of apatite deposits after incubation in SBF. From the results of in vitro biological assay, it is concluded that the synergetic effect of BR and GPTMS provided an enhanced hFob cells attachment and proliferation. The developed PHBV/G-BR nanofibrous scaffolds may be considered for application in bone tissue engineering.

Keywords Bredigite nanoparticles · PHBV · GPTMS · Electrospinning · Bone tissue engineering

✉ Monireh Kouhi
monireh.kouhi@ma.iut.ac.ir

¹ Biomaterials Research Group, Department of Materials Engineering, Isfahan University of Technology, Isfahan 8415683111, Iran

² Center for Nanofibers and Nanotechnology, Department of Mechanical Engineering, National University of Singapore, Singapore 117576, Singapore

³ Faculty of Industrial Sciences and Technology, Universiti Malaysia Pahang, 26300 Gambang, Kuantan, Pahang, Malaysia

Introduction

The native bone tissue extracellular matrix (ECM) is mainly composed of carbonated apatite nanocrystals (2–5 nm wide and 70 nm long) and collagen type I fibrous matrix (50–500-nm diameter) [1–3]. Considering the structural features of bone ECM, nanofibrous materials containing bioceramic nanoparticles can be served as ideal scaffolding materials for promoting osteoblast proliferation and infiltration in bone tissue engineering applications. Till date, different methods such as drawing, thermally induced phase separation, molecular self-assembly, and electrospinning have been introduced and studied to produce nanofibers. Among them, electrospinning is the most widely applied technique for generating nanoparticles embedded nanofibrous scaffolds due to its ease of use and relatively low-cost instrumental setup [4–6].

Poly (3-hydroxybutyrate-co-3-hydroxyvalerate) (PHBV), a member of the polyhydroxyalkanoates family, is the copolymer of polyhydroxybutyrate and polyhydroxyvalerate which has been reported to promote bone growth *in vivo*, because of its piezoelectric properties. In addition, it decomposes to 3-hydroxybutyric acid, a normal constituent of blood which increases calcium influx to the cells and prevents cells death. This makes the polymer highly biocompatible and non-toxic for application as scaffolding materials for bone tissue engineering applications [7–9].

Previous studies have demonstrated that Mg-Ca-Si-based bioceramics possessed superior apatite-mineralization ability, biocompatibility, and biological properties compared to calcium phosphate bioceramics. Bredigite ($\text{Ca}_7\text{MgSi}_4\text{O}_{16}$) is belonging to this category which is found to have great cytocompatibility, a highly stimulating effect on osteoblast proliferation and osteogenic differentiation potential [10–13]. In our previous work, bredigite nanoparticles were synthesized using the sol–gel method and incorporated into PHBV nanofibers through electrospinning. Our results revealed that addition of bredigite nanoparticles more than 10% resulted in the production of uneven nanofibers with reduced mechanical properties due to the particle agglomeration [4, 14]. When hydrophilic nanoparticles are applied in combination with hydrophobic polymers, a main problem usually emerged, that is the inhomogeneous dispersion of the nanoparticles in the matrix. Nano-size particles with an enormous surface area and high surface energy tend to agglomerate in polymer matrix due to the weak interface between the nanoparticles and polymer matrix. This aggregation and incompatibility would become the origin of the early failure, which decreases the mechanical performance of the composites and prevents cell attachment/proliferation and protein adsorption [15–17]. To improve the compatibility and dispersibility of inorganic nanoparticles, different organic modifiers, such as cetyl trimethylammonium bromide [18], polyethylene glycol [19], dodecyl alcohol [20], and stearic acid [21], were applied and investigated. However, these modifiers exhibited some disadvantages such as weak binding to the nanoparticles, reduction in the hydrophilicity, and having cytotoxicity effect, which make them unsuitable for preparing tissue engineering scaffolds [16, 17]. In the present study, we utilized 3-glycidioxypropyltrimethoxysilane (GPTMS) as a coupling agent to improve the dispersion of bredigite nanoparticles within the PHBV matrix. In a study by Li et al. [22], the pretreating of hydroxyapatite nanoparticles with GPTMS was reported. Their results showed improved nanoparticle dispersion in polycaprolactone matrix. It was also demonstrated that mechanical properties and bioactivity of the scaffolds were highly improved by applying modified nanoparticles.

In the current research work, bredigite nanoparticles were modified with GPTMS and loaded into PHBV nanofibers using electrospinning. Resultant PHBV nanofibrous scaffolds were characterized and their mechanical properties and apatite-forming ability were evaluated. Finally, hFob cells were cultured on the composite scaffolds to assay cell–scaffold interaction for bone tissue engineering applications.

Materials and Methods

Surface Modification of Bredigite Nanoparticles

Bredigite (BR) nanoparticles obtained from our previous work [23] were mixed with GPTMS (Sigma–Aldrich) solution in ethanol (1:50 *v/v*) followed by a stirring at 60 °C for 2 h. The temperature was then raised up to 75 °C to evaporate ethanol and the GPTMS-modified bredigite (G-BR) nanoparticles were dried for 24 h at 120 °C under vacuum. The modification process is schematically given in Fig. 1. To investigate the chemical composition of BR and G-BR nanoparticles, Fourier transform infrared (FTIR) spectrometer (Avatar 380 - ThermoQ14 Nicolet, MA) was utilized at a resolution of 4 cm^{-1} and a spectra range of 4000–400 cm^{-1} .

Electrospinning of Composite Nanofibers

Electrospun PHBV/BR and PHBV/G-BR nanofibers were developed according to our previous study [4]. Briefly, the desired amount of BR and G-BR nanoparticles was sonicated in 1,1,1,3,3,3 hexafluoro-2-propanol (Sigma) for 30 min, and then PHBV (HV content 3%, Mw: 400000, TianAn Enmat Chemical Company, China) was added to the obtained mixture to get a 8 wt% polymer solution, and stirred at room temperature overnight. The prepared solutions were subjected to an electrospinning setup made of a high voltage (Gamma High Voltage Research, FL, USA), a syringe pump (KD 100 Scientific Inc., Holliston, MA, USA), and a collector. Electrospinning was performed at the flow rate of 1 ml/h, a high voltage of 14 kV, and working distance of 18 cm. The produced nanofibers were dried at room temperature for 24 h and kept in desiccator for further tests.

Morphological Characterization of the Nanofibers

Field emission scanning microscopy (FESEM: HITACHI S-4300, Japan) was employed to observe and study the morphology of electrospun nanofiber. The diameter of the obtained nanofiber was determined from FESEM images using ImageJ software (Image Java, National Institutes of Health, Bethesda, MD, USA). Transmission electron microscopy (TEM, Philips CM-120) was used to observe the nanoparticle distribution and agglomeration within the composite nanofiber.

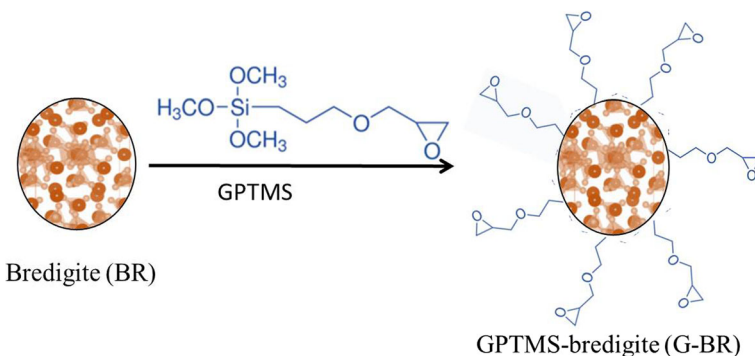


Fig. 1 Schematic of surface modification of bredigite nanoparticles

Mechanical Characterization of the Nanofibrous Scaffolds

For the mechanical characterization of the nanofibrous scaffolds, rectangular strips ($10 \times 20 \text{ mm}^2$) of the scaffolds were mounted vertically on the gripping unit of a tabletop tensile tester (Instron 5943, USA) and tested with a load cell of 50 N at a crosshead of 10 mm/min. Tensile properties of the samples including tensile strength, Young modulus, and elongation at break were calculated from the stress–strain curves. The test was repeated five times for each specimen and the data was reported as the mean and standard deviation.

In Vitro Bioactivity Evaluation

Bone-like apatite-forming ability of the nanofibrous scaffolds was examined by immersion the samples into the simulated body fluid (SBF) solution with the ion concentration similar to those of the human body. Nanofibrous scaffolds of $10 \times 10 \text{ mm}^2$ were soaked in 30 ml of SBF solution in polyethylene bottle at 37°C and pH of 7.4 for the predetermined time period and then were washed with DI water, dried and subjected to SEM coupled with energy dispersive spectroscopy (SEM–EDS) for further characterization. The formation of apatite layer on the surface of composite nanofibrous scaffolds was confirmed by X-ray diffractometer (XRD) (Philips X'Pert-MPD, Cu Ka radiation at 30 mA and 40 kV, at a scan rate of $3^\circ/\text{min}$). Ion concentration of the SBF solution during bioactivity test was determined using inductively coupled plasma atomic emission spectroscopy (ICP-OES, Perkin-Elmer Optima 7300DV).

In Vitro Cellular Assay

Cell Culture

The hFob cells, obtained from the American Type Culture Collection (ATCC, VA 20108, USA), were cultured in Dulbecco's modified eagles medium/nutrient mixture F-12 (DMEM/F12, Sigma–Aldrich, Singapore), supplemented with 10% fetal bovine serum (FBS, GIBCO, Invitrogen Corp, USA) and 1% antibiotic solution (Sigma–Aldrich, A5955), and incubated in CO_2 incubator at 37°C and 5% CO_2 . After confluency, cells were detached by trypsin/EDTA (GIBCO, Invitrogen Corp, USA) and seeded on the nanofibrous scaffolds at the seeding density of 10,000 cells/well. To study cell–scaffold interactions, the nanofibrous scaffolds were placed in a 24-well plate and pressed with stainless steel rings. The scaffolds were then sterilized using UV light for 2 h, washed three times with PBS, and immersed in complete medium (DMEM/F12-10% FBS-1% antibiotics) overnight before culturing of cells.

Cell Proliferation

The hFob proliferation on the electrospun scaffolds was evaluated using the colorimetric MTS assay (CellTiter 96 Aqueous One solution; Promega, Madison, USA) at 490 nm. After 5, 10, and 15 days of cell culture, the media was discarded from the wells and the scaffolds were rinsed with PBS and incubated with MTS reagent (20%) in serum-free medium in 5% CO_2 incubator at 37°C for 3 h. After the incubation period, the obtained dye was aliquoted into 96-well plates and read using a spectrophotometric plate reader (FLUO star OPTIMA, BMG Lab Technologies, Germany). The experiments were repeated three times and the cells grown on tissue culture plastic (TCP) served as the control.

Cell Morphology Study

The morphology of the hFob cells cultured on the different samples was evaluated using FESEM. After 5 and 15 days of the cell culture, the media was discarded from the wells and the samples were rinsed with PBS and fixed with glutaraldehyde in PBS (3%) for 3 h. The scaffolds with cells were then rinsed with distilled water for 15 min and dehydrated with a series of ethanol solutions of increasing concentrations (30%, 50%, 75%, 90%, and 100% (v/v)), finally treated with hexamethyldisilazane (HMDS, Sigma–Aldrich), and left to dry overnight at ambient temperature. The dried samples were observed under FESEM.

Statistical Analysis

All data are shown as means and standard deviation. Statistical significance was evaluated using a one-way analysis of variance (ANOVA) with pairwise comparisons made by Tukey's post hoc analysis. The significant differences were indicated at $P < 0.05$.

Results and Discussion

Characterization of Nanoparticles and Nanofibrous Scaffolds

Figure 2a, b shows the SEM and TEM images of BR nanoparticles which appear to be irregular particles with size ranging from 25 to 50 nm that tend to agglomerate. The successful modification of BR nanoparticles with GPTMS was confirmed by FTIR spectroscopy. Figure 2c shows the FTIR spectra of BR and G-BR nanoparticles. The spectra for BR nanoparticles show the characteristic peaks of bredigite including SiO_4 stretching bond at $1000\text{--}1100\text{ cm}^{-1}$ and 869 cm^{-1} , SiO_4 bending bond at 620 cm^{-1} and 460 cm^{-1} , Mg–O bond at 475 cm^{-1} , and Ca–O stretching bond at 533 cm^{-1} [23, 24]. On modification with GPTMS, the peaks at 911 cm^{-1} and 1090 cm^{-1} corresponding to the epoxy group and Si–OCH₃ bond, respectively, were appeared or their intensity increased, confirming the presence of GPTMS on the surface of bredigite [25–27]. Figure 3 shows the SEM images of the pure PHBV and PHBV nanofibers containing 5% and 15% of either BR or G-BR nanoparticles. The mean fiber diameter of the pure and composite PHBV nanofibers is given in Table 1. Continuous and relatively even nanofibers were successfully obtained for pure PHBV and composite PHBV nanofibers containing 5% of either BR or G-BR

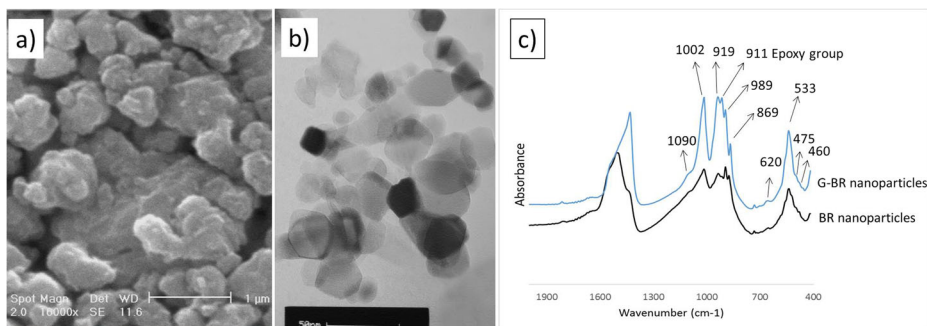


Fig. 2 SEM image of BR nanoparticles (a), TEM image of BR nanoparticles (b), and FTIR spectra of BR and G-BR nanoparticles (c)

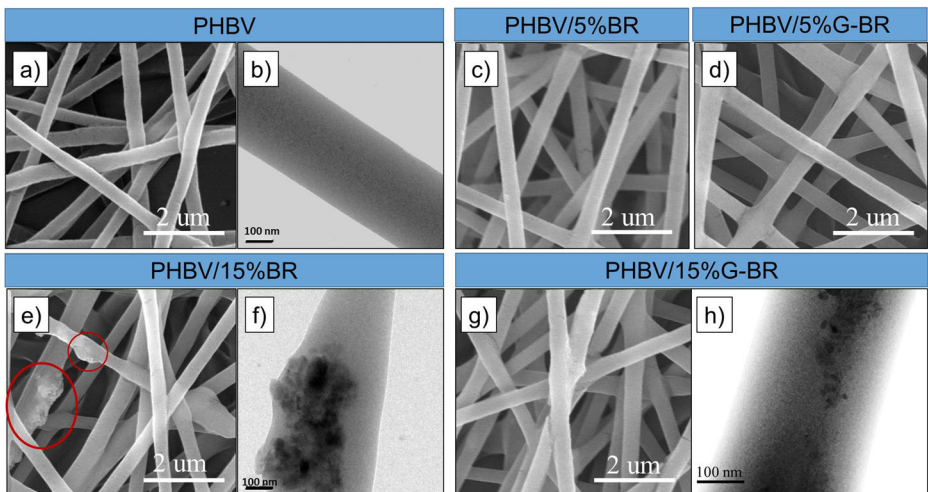


Fig. 3 SEM images of pure PHBV (a), PHBV/5%BR (c), PHBV/5%G-BR (d), PHBV/15%BR (red circles indicate the nanoparticles' agglomerates) (e), and PHBV/15%G-BR (g) nanofibrous scaffolds and TEM images of pure PHBV (b), PHBV/15%BR (f), and PHBV/15%G-BR (h) nanofibers

nanoparticles. A slight increase in mean fiber diameter was observed by incorporation of nanoparticles. By increasing the concentration of BR nanoparticles to 15%, a sign of agglomeration was observed for BR nanoparticles embedded nanofiber; however, PHBV composite nanofibers containing 15% G-BR nanoparticles showed the relatively better dispersion of nanoparticles as a result of GPTMS modification. This observation was then confirmed by TEM analysis as given in Fig. 3. TEM images show that G-BR nanoparticles dispersed more homogenous than BR nanoparticles within PHBV nanofibers.

The mechanical performance of the nanofibrous structures incorporated with nanoparticles is highly affected by the particle dispersion state. The mechanical properties of PHBV nanofibrous scaffolds were evaluated by their Young's modulus, ultimate strength, and strain at break. Figure 4 shows the stress–strain curves for PHBV, PHBV/5%BR, PHBV/15%BR, PHBV/5%G-BR, and PHBV/15%G-BR scaffolds, along with the mechanical properties of different scaffolds. Young's modulus, ultimate strength, and strain at break of the nanofibrous samples are summarized in Table 1. All stress–strain curves exhibited a similar trend with remarkable changes in mechanical properties depending on bredigite concentration and its dispersion state within the PHBV scaffolds. As evident from the results, by incorporation of 5% nanoparticles, Young's modulus and ultimate strength of PHBV scaffolds (106.7 MPa and 4.41 MPa, respectively) were significantly increased to 147.3 MPa and 4.9 MPa for PHBV/5%BR, and to 150.1 MPa and 5.2 MPa for PHBV/5%G-BR,

Table 1 Average fiber diameter and the mechanical properties of different nanofibrous scaffolds

	Average fiber diameter (nm)	Young's modulus (MPa)	Ultimate strength (MPa)	Elongation at break (%)
PHBV	359 ± 30	106.7 ± 31.3	4.41 ± 0.27	64.61 ± 22.78
PHBV/5%BR	378 ± 19	147.3 ± 33.2	4.96 ± 0.69	54.49 ± 7.78
PHBV/5%G-BR	389 ± 24	150.1 ± 10.1	5.20 ± 0.49	58.61 ± 10.24
PHBV/15%BR	361 ± 73	105.6 ± 34.6	3.87 ± 0.38	39.83 ± 11.38
PHBV/15%G-BR	393 ± 14	175 ± 25.6	6.36 ± 0.54	60.76 ± 5.21
PHBV/20%G-BR	397 ± 85	183.4 ± 41.1	6.52 ± 0.21	57.26 ± 15.3

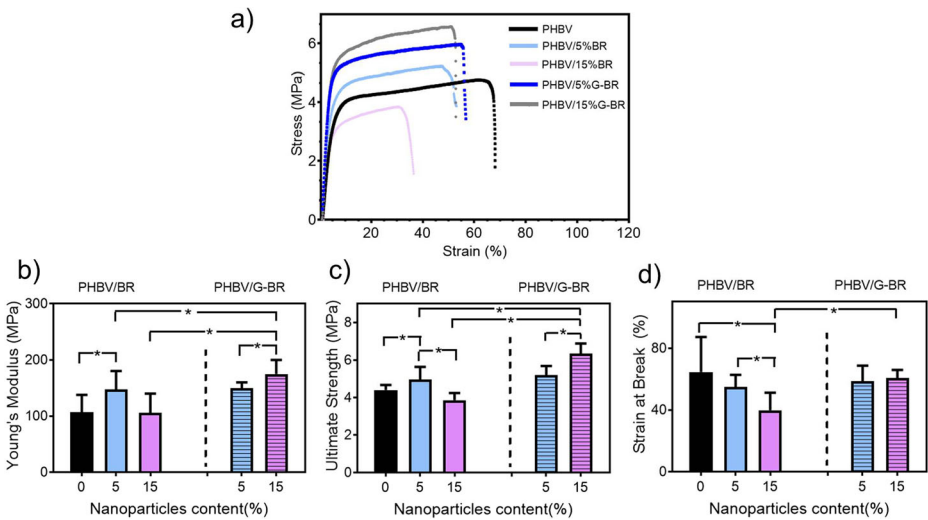


Fig. 4 Stress–strain curves of pure and composite PHBV nanofibrous scaffolds (a), and mechanical properties of the PHBV nanofibrous scaffolds, Young's modulus (b), ultimate strength (c), and strain at break (d) (*significant difference between the group at $P < 0.05$)

due to reinforcement effect of nanoparticles; however, elongation at break decreased from 64.6% for PHBV scaffold to 54.5% (PHBV/5%BR) and 58.6% (PHBV/5%G-BR), indicating higher resistance to deformation. This behavior can be attributed to the bredigite stiffness which decreased the flexibility of the PHBV composite scaffolds. According to Fig. 4, at higher concentration of nanoparticles (15%), the PHBV/15%BR scaffolds exhibited lower Young's modulus and ultimate strength compared to all other PHBV scaffolds, because of the nanoparticle agglomeration and concentrated stress on the agglomerates. Such a reduction in the mechanical properties of the composite nanofibrous structures by increasing the particle concentration has been reported previously in the literature [22, 28]. By incorporation of 15% G-BR nanoparticles, strength and modulus of PHBV composite scaffold was significantly increased compared to pure PHBV and PHBV/15%BR scaffolds ($P \leq 0.05$), due to the better dispersion of the G-BR nanoparticles within PHBV matrix which allows better transference of concentrated stress from the matrix to nanoparticles. These findings suggest that GPTMS treatment is beneficial in improving the mechanical performance of PHBV composite scaffolds at higher concentration of nanoparticles.

In Vitro Bioactivity Evaluation

In vitro bone-like mineral-forming ability at the material surface is thought to be an important property of scaffolds for bone tissue engineering applications, which were examined by immersion test in SBF during this research. Figure 5 shows the morphological changes of the pure and composite PHBV scaffolds containing 15% either BR or G-BR nanoparticles after incubation for 2 and 4 weeks. After 2-week incubation in SBF, the formation of apatite mineral deposits on the PHBV nanofibers containing nanoparticles was evidence which was grown to the flower-like structures and covered the entire surface of the nanofibers at prolonged incubation time (4 weeks), while pure PHBV nanofibers did not induce the formation of apatite minerals after 4 weeks. As reported in the literature, ceramic and glass-ceramic biomaterials containing CaO-SiO_2 can induce apatite nucleation and growth through the formed silanol group (Si-OH) as a result of Si-O-Si bonds breakage [4]. Morphological features of the formed deposits on PHBV/BR and PHBV/G-BR

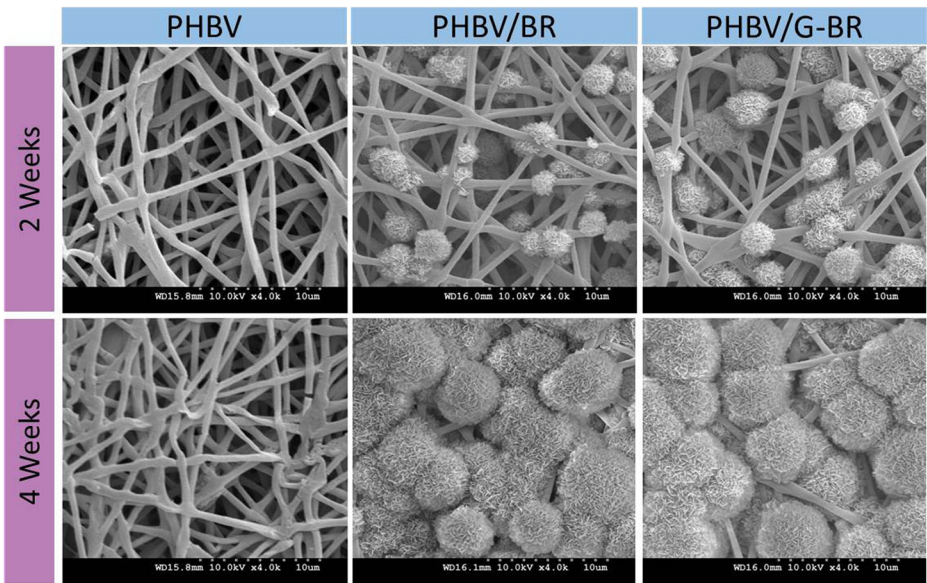


Fig. 5 SEM images of PHBV, PHBV/BR, and PHBV/G-BR nanofibrous scaffolds after 2- and 4-week incubation in SBF

nanofiber surfaces were similar, indicating that scaffolds remained still bioactive after surface modification with GPTMS. Figure 6 shows the results of EDS analysis on the surface of nanofibrous scaffolds after 4 weeks incubation in SBF. According to the EDS results, the newly formed materials are mainly composed of calcium and phosphorous, which were further characterized by XRD analysis (Fig. 7). In the XRD pattern of all samples, several diffraction peaks at around 14, 17, 20, 22, and 27.5 degrees can be observed which could be assigned to the crystalline structure of PHBV [29, 30]. In the XRD pattern of PHBV/BR and PHBV/G-BR, the presence of two peaks at around 26 and 32 degrees confirmed the formation of crystalline apatite on the surface of composite nanofibers after incubation in SBF. The results of EDS and XRD analysis together with the SEM observation revealed that PHBV nanofibrous scaffolds incorporated with either BR or G-BR nanoparticles have the ability to produce bone-like apatite layer on their surface during incubation in SBF.

Figure 8 shows the changes in silicon (Si), calcium (Ca), and phosphorous (P) ion concentration in SBF containing composite PHBV nanofibers after 4-week incubation of samples, which was determined by ICP analysis. Results showed that Si concentrations in SBF increased with

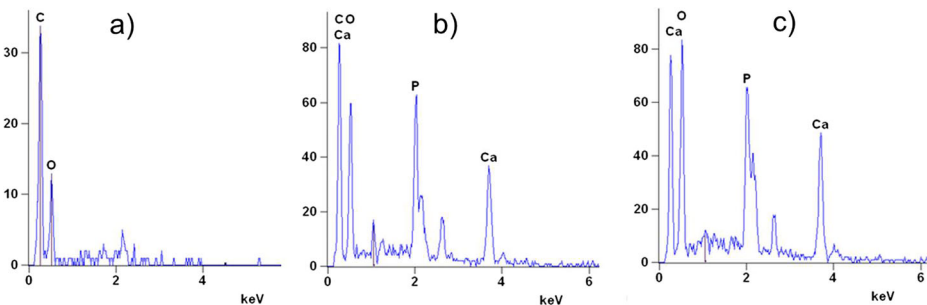


Fig. 6 EDS analysis of the surface of nanofibrous scaffolds after incubation in SBF for 4 weeks: **a** PHBV, **b** PHBV/BR, and **c** PHBV/G-BR

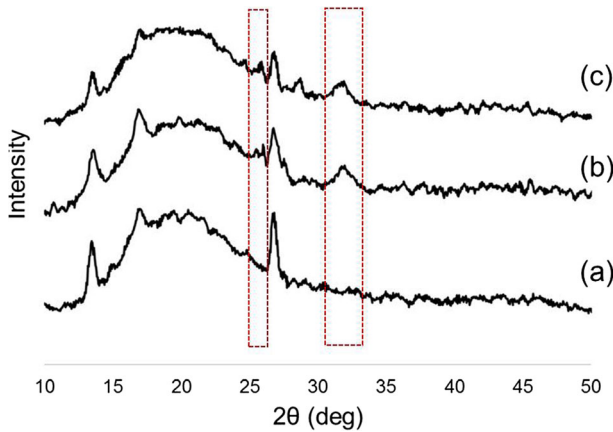


Fig. 7 XRD patterns of different samples after incubation in SBF for 4 weeks: (a) PHBV, (b) PHBV/BR, and (c) PHBV/G-BR

increasing soaking time, which was attributed to the dissolution of the Si ion from the bredigite. The concentration of P ion in SBF decreased during incubation, due to the P consumption from the SBF solution toward the surface of the samples to form and growth of apatite deposits. The trend in Ca concentration showed an increase in the beginning due to the dissolution of the Ca into the SBF, followed by a decrease during immersion test, due to the formation of Ca-P layer on the surface of the samples. The formation and growth of Ca-P nuclei cause the formation of apatite layer which consumes the Ca and P ions from the surrounding liquid [31, 32], resulting in the observed decrease in Ca and P concentration in SBF solution. Compared to BR nanoparticles, G-BR nanoparticles embedded nanofibers consumed more Ca and P ions from the solution which might be due to the presence of silanol groups on the surface of modified nanoparticles, which increased nucleation sites for the formation of apatite minerals [3].

In Vitro Cellular Assay

The proliferation of hFob cells on the different scaffolds was evaluated using colorimetric MTS assay. Figure 9 shows the results of MTS assay on different nanofibrous scaffolds and control sample, which demonstrated that all samples got the upward trend, indicating that cells grew on the surface of all substrates. The hFob cultured on pure PHBV scaffold showed the lower proliferation compared to composite PHBV scaffolds and TCP. Biomaterials with hydrophobic nature exhibit a lower cell adhesion and proliferation [33]. By incorporating either BR or G-BR nanoparticles into PHBV nanofibers, the proliferation of hFob cells enhanced by 22% and 35%, respectively, after 5 days of cell culture. As reported in the previous studies, silicate-based bioceramics could stimulate

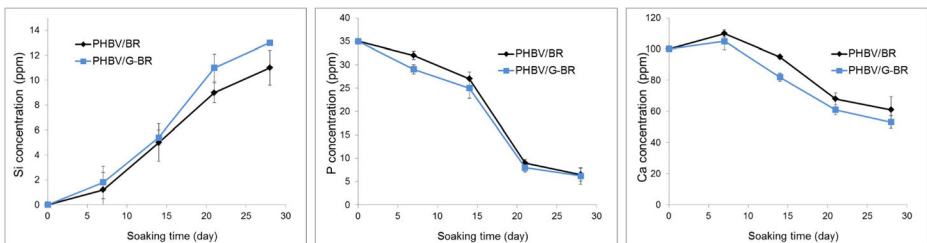


Fig. 8 The changes in Si, P, and Ca ion concentrations in SBF solution during incubation of the scaffolds for 4 weeks

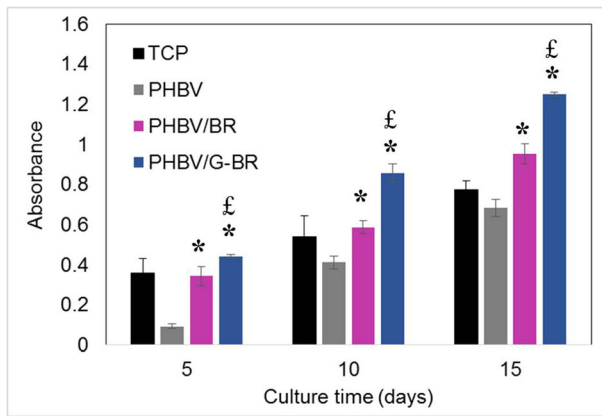


Fig. 9 Proliferation of hFob cells determined by MTS assay on PHBV, PHBV/BR, and PHBV/G-BR nanofibrous scaffolds and TCP on days 5, 10, and 15 (*significant difference relative to PHBV scaffold ($P < 0.05$), £: significant difference relative to PHBV/BR scaffold ($P < 0.05$))

the osteoblasts cell adhesion, spreading and proliferation through releasing the Si-containing ionic products [34, 35]. Results of cell proliferation study also demonstrated that PHBV/G-BR scaffolds presented significantly higher hFob proliferation than PHBV/BR scaffolds by 27% and 33% after 10 and 15 days of cell culture, respectively. It has been reported that Si-OH and -Si-O-Si-groups of GPTSM have an important effect on osteoblast proliferation since Si ions are known to influence the activity of bone cells [36]. Therefore, it is concluded that the synergetic effect of BR and GPTMS provided an enhanced cell attachment and growth.

Cellular morphology of the hFob cells seeded on PHBV, PHBV/BR, PHBV/G-BR, and control samples were visualized by FESEM (Fig. 10) after 5 and 15 days of cell seeding. On day 5, the hFob cells tethered to the surface of all nanofibrous scaffolds with flattened and polygonal extensions; however, the cells apparently spread and grew better on composite PHBV scaffolds compared to pure PHBV and control sample. After 15 days of cell culture, the surface of PHBV composite scaffolds was completely covered by a thick layer of cells with the formation of mineral deposits revealing the confluent cell growth and cell-secreted mineralization. Overall results demonstrated that incorporation of G-BR nanoparticles instead of BR nanoparticles into the PHBV nanofibrous scaffolds enabled them to possess better microarchitecture as a result of better dispersibility, improved mechanical properties, and enhanced biological performance.

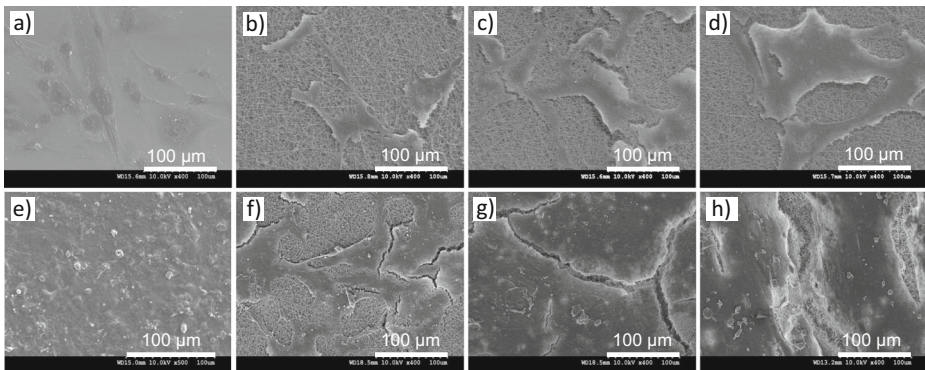


Fig. 10 SEM images of hFob cells cultured on TCP (a, e), PHBV (b, f), PHBV/BR (c, g), and PHBV/G-BR (d, i) scaffolds on days 5 (a–d) and 15 (e–h), representing the cell growth and mineralization

Conclusion

In this research, bredigite nanoparticles were modified with GPTMS and incorporated into PHBV nanofibers through electrospinning technique. On modification with GPTMS, the better dispersion state of BR nanoparticles within the PHBV matrix was obtained, which resulted in the production of composite nanofibers with homogenous and even structures. Incorporation of modified BR nanoparticles significantly improved the strength and modulus of PHBV composite scaffold compared to pure PHBV and PHBV containing unmodified BR, especially at the higher concentration of nanoparticles. The fabricated PHBV/G-BR nanofibrous scaffold was in vitro bioactive, the apatite deposits were observed on the fiber surface after soaking in SBF. Moreover, the in vitro cellular assay revealed that PHBV/G-BR scaffold exhibited enhanced hFob cell attachment and proliferation compared to PHBV/BR, suggesting its greater potential for bone tissue engineering application.

Compliance with Ethical Standards

Conflict of Interest The authors declare that they have no conflict of interest.

References

1. Talebian, S., Mehrali, M., Mohan, S., Balajiraghavendran, H., Mehrali, M., Khanlou, H. M., et al. (2014). Chitosan (PEO)/bioactive glass hybrid nanofibers for bone tissue engineering. *RSC Advances*, 4(90), 49144–49152.
2. Holzwarth, J. M., & Ma, P. X. (2011). Biomimetic nanofibrous scaffolds for bone tissue engineering. *Biomaterials*, 32(36), 9622–9629.
3. Tahriri, M., & Moztarzadeh, F. (2014). Preparation, characterization, and in vitro biological evaluation of PLGA/nano-fluorohydroxyapatite (FHA) microsphere-sintered scaffolds for biomedical applications. *Applied Biochemistry and Biotechnology*, 172(5), 2465–2479.
4. Kouhi, M., Prabhakaran, M. P., Shamanian, M., Fathi, M., Morshed, M., & Ramakrishna, S. (2015). Electrospun PHBV nanofibers containing HA and bredigite nanoparticles: fabrication, characterization and evaluation of mechanical properties and bioactivity. *Composites Science and Technology*, 121, 115–122.
5. Venugopal, J., & Ramakrishna, S. (2005). Applications of polymer nanofibers in biomedicine and biotechnology. *Applied Biochemistry and Biotechnology*, 125(3), 147–157.
6. Saadatkish, N., Nouri Khorasani, S., Morshed, M., Allafchian, A.-R., Beigi, M.-H., Masoudi Rad, M., Esmacely Neisiany, R., & Nasr-Esfahani, M. H. (2018). A ternary nanofibrous scaffold potential for central nerve system tissue engineering. *Journal of Biomedical Materials Research Part A*, 106(9), 2394–2401.
7. Ansari, N. F., & Amirul, A. A. (2013). Preparation and characterization of polyhydroxyalkanoates macroporous scaffold through enzyme-mediated modifications. *Applied Biochemistry and Biotechnology*, 170(3), 690–709.
8. Zhao, Y., Zou, B., Shi, Z., Wu, Q., & Chen, G.-Q. (2007). The effect of 3-hydroxybutyrate on the in vitro differentiation of murine osteoblast MC3T3-E1 and in vivo bone formation in ovariectomized rats. *Biomaterials*, 28(20), 3063–3073.
9. Kouhi, M., Fathi, M., Venugopal, J. R., Shamanian, M., & Ramakrishna, S. (2018). Preparation and characterization of biohybrid poly (3-hydroxybutyrate-co-3-hydroxyvalerate) based nanofibrous scaffolds. *AIP Conference Proceedings*, 1920, 020014.
10. Dezfūli, S. N., Huan, Z., Mol, A., Leeftang, S., Chang, J., & Zhou, J. (2017). Advanced bredigite-containing magnesium-matrix composites for biodegradable bone implant applications. *Materials Science and Engineering C*, 79, 647–660.
11. Rahmati, M., Fathi, M., & Ahmadian, M. (2018). Preparation and structural characterization of bioactive bredigite (Ca₇MgSi₄O₁₆) nanopowder. *Journal of Alloys and Compounds*, 732, 9–15.
12. Khandan, A., Ozada, N., Saber-Samandari, S., & Ghadiri Nejad, M. (2018). On the mechanical and biological properties of bredigite-magnetite (Ca₇MgSi₄O₁₆-Fe₃O₄) nanocomposite scaffolds. *Ceramics International*, 44(3), 3141–3148.
13. Zhou, Y., Wu, C., & Xiao, Y. (2014). Silicate-based bioceramics for periodontal regeneration. *Journal of Materials Chemistry B*, 2(25), 3907–3910.

14. Kouhi, M., Fathi, M., Prabhakaran, M. P., Shamanian, M., & Ramakrishna, S. (2018). Enhanced proliferation and mineralization of human fetal osteoblast cells on PHBV-bredigite nanofibrous scaffolds. *Materials Today: Proceedings*, 5(7), 15702–15709.
15. Diao, H., Si, Y., Zhu, A., Ji, L., & Shi, H. (2012). Surface modified nano-hydroxyapatite/poly (lactide acid) composite and its osteocyte compatibility. *Materials Science and Engineering: C*, 32(7), 1796–1801.
16. Zhang, M., Ye, L., Gao, Y., Lv, X., & Chang, J. (2009). Effects of hydrolysis on dodecyl alcohol modified β -CaSiO₃ particles and PDLA/modified β -CaSiO₃ composite films. *Composites Science and Technology*, 69(15–16), 2547–2553.
17. Wang, D., Xuan, L., Zhong, H., Gong, Y., Shi, X., Ye, F., Li, Y., & Jiang, Q. (2017). Incorporation of well-dispersed calcium phosphate nanoparticles into PLGA electrospun nanofibers to enhance the osteogenic induction potential. *RSC Advances*, 7(39), 23982–23993.
18. El-Fiqi, A., Kim, T.-H., Kim, M., Eltohamy, M., Won, J.-E., Lee, E.-J., et al. (2012). Capacity of mesoporous bioactive glass nanoparticles to deliver therapeutic molecules. *Nanoscale*, 4(23), 7475–7488.
19. Hong, Z., Reis, R. L., & Mano, J. F. (2009). Preparation and in vitro characterization of novel bioactive glass ceramic nanoparticles. *Journal of Biomedical Materials Research Part A*, 88A(2), 304–313.
20. Borum-Nicholas, L., & Wilson, O. C. (2003). Surface modification of hydroxyapatite. Part I. Dodecyl alcohol. *Biomaterials*, 24(21), 3671–3679.
21. Li, Y., & Weng, W. (2008). Surface modification of hydroxyapatite by stearic acid: characterization and in vitro behaviors. *Journal of Materials Science: Materials in Medicine*, 19(1), 19–25.
22. Li, L., Li, G., Jiang, J., Liu, X., Luo, L., & Nan, K. (2012). Electrospun fibrous scaffold of hydroxyapatite/poly (ϵ -caprolactone) for bone regeneration. *Journal of Materials Science: Materials in Medicine*, 23(2), 547–554.
23. Kouhi, M., Shamanian, M., Fathi, M., Samadikuchaksaraei, A., & Mehdipour, A. (2016). Synthesis, characterization, in vitro bioactivity and biocompatibility evaluation of hydroxyapatite/bredigite (Ca₇MgSi₄O₁₆) composite nanoparticles. *JOM*, 68(4), 1061–1070.
24. Mirhadi, S. M., Tavangarian, F., & Emadi, R. (2012). Synthesis, characterization and formation mechanism of single-phase nanostructure bredigite powder. *Materials Science and Engineering: C*, 32(2), 133–139.
25. Tarik Arafat, M., Lam, C. X. F., Ekaputra, A. K., Wong, S. Y., He, C., Hutmacher, D. W., Li, X., & Gibson, I. (2011). High performance additive manufactured scaffolds for bone tissue engineering application. *Soft Matter*, 7(18), 8013.
26. Yuan, J., Zhou, S., Gu, G., & Wu, L. (2005). Effect of the particle size of nanosilica on the performance of epoxy/silica composite coatings. *Journal of Materials Science*, 40(15), 3927–3932.
27. Zhang, Q., RongFu, H., Liang-Hong, G. (2009). One-step and high-density protein immobilization on epoxysilane-modified silica nanoparticles. *Chinese Science Bulletin*, 54.
28. Kim, H., Che, L., Ha, Y., & Ryu, W. H. (2014). Mechanically-reinforced electrospun composite silk fibroin nanofibers containing hydroxyapatite nanoparticles. *Materials Science and Engineering C*, 40, 324–335.
29. Xu, Y., Zou, L., Lu, H., Wei, Y., Hua, J., & Chen, S. (2016). Preparation and characterization of electrospun PHBV/PEO mats: the role of solvent and PEO component. *Journal of Materials Science*, 51(12), 5695–5711.
30. Tadokoro, H., Chatani, Y., & Yoshihara, T. (1964). Structural studies on polyethers, [-(CH₂)_m-O]-_n. II. Molecular structure of polyethylene oxide. *Macromolecular Chemistry and Physics*, 73, 109–127.
31. Ashuri, M., Moztarzadeh, F., Nezafati, N., Ansari Hamedani, A., & Tahiri, M. (2012). Development of a composite based on hydroxyapatite and magnesium and zinc-containing sol-gel-derived bioactive glass for bone substitute applications. *Materials Science and Engineering: C*, 32(8), 2330–2339.
32. Ghomi, H., Fathi, M. H., & Edris, H. (2011). Preparation of nanostructure hydroxyapatite scaffold for tissue engineering applications. *Journal of Sol-Gel Science and Technology*, 58(3), 642–650.
33. Rajzer, I., Menaszek, E., Kwiatkowski, R., Planell, J. A., & Castano, O. (2014). Electrospun gelatin/poly(ϵ -caprolactone) fibrous scaffold modified with calcium phosphate for bone tissue engineering. *Materials Science and Engineering: C*, 44, 183–190.
34. Kouhi, M., Fathi, M., Prabhakaran, M. P., Shamanian, M., & Ramakrishna, S. (2018). Poly L lysine-modified PHBV based nanofibrous scaffolds for bone cell mineralization and osteogenic differentiation. *Applied Surface Science*, 457, 616–625.
35. Wu, C., & Chang, J. (2007). Degradation, bioactivity, and cytocompatibility of diopside, akermanite, and bredigite ceramics. *Journal of Biomedical Materials Research Part B: Applied Biomaterials*, 83B(1), 153–160.
36. Shirotsaki, Y., Tsuru, K., Hayakawa, S., Osaka, A., Lopes, M. A., Santos, J. D., & Fernandes, M. H. (2005). In vitro cytocompatibility of MG63 cells on chitosan-organosiloxane hybrid membranes. *Biomaterials*, 26(5), 485–493.